Electronic Supplementary Material (ESI) for Lab on a Chip.


# Supplementary Information:

# Investigation of different nanoparticles for magnetophoretically enabled nanofin heat sinks in microfluidics

Pyshar Yi, [*a] Khashayar Khoshmanesh,[*a] Jos L. Campbell,[b] Phillip Coughlan,[a]

Kamran Ghorbani,[a] and Kourosh Kalantar-zadeh[*a]

[a] RMIT University, School of Electrical and Computer Engineering, Melbourne, Victoria 3001, Australia.

[b] School of Applied Sciences, RMIT University, Melbourne, Victoria 3001, Australia.

E-mail: pyshar.yi@gmail.com,

kourosh.kalantar@rmit.edu.au,

khashayar.khoshmanesh@rmit.edu.au

**Supplementary Information 1: Apparatus**

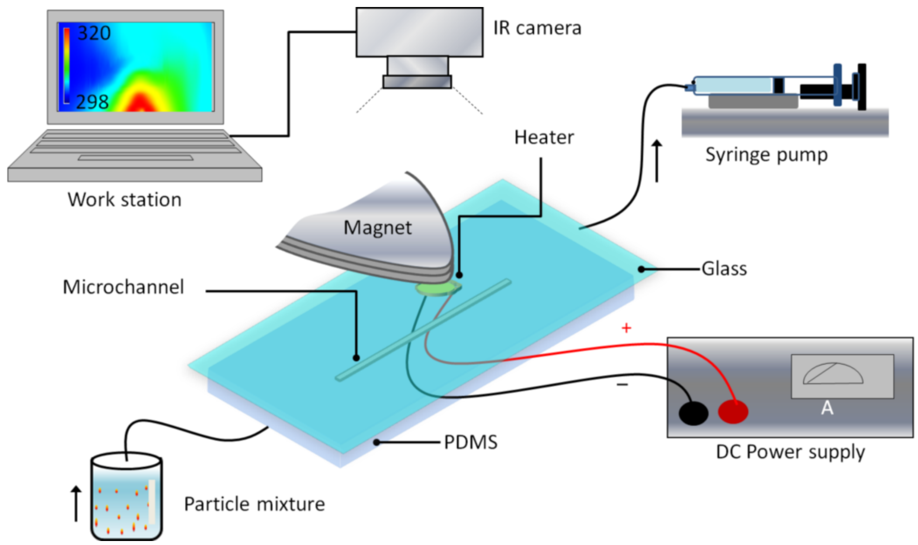


**Fig. S1** Experimental setup for thermal characterizations of the microfluidic system.

**Supplementary Information 2: Thermophysical properties of suspensions**

To calculate the values of $\rho_{suspension}$ , $\mu_{suspension}$, $c_{p\text{-}suspension}$ and and $k_{suspension}$ for the DI water, $CrO_2$ suspension, and $Fe_2O_3$ suspension, we use the following equations[1]:

$$\rho_{suspension} = (1-\phi)\rho_f + \phi\rho_p \tag{1}$$

$$\mu_{suspension} = \frac{1}{(1-\phi)^{2.5}}\mu_f \tag{2}$$

$$(\rho c_p)_{suspension} = (1-\phi)(\rho c_p)_f + \phi(\rho c_p)_p \tag{3}$$

$$k_{suspension} = \frac{k_p + (n-1)k_f - (n-1)\phi(k_f - k_p)}{k_p + (n-1)k_f + \phi(k_f - k_p)} k_f \tag{4}$$

where $f$ and $p$ indices refer to fluid and particle, respectively. $Ø$ is the volume fraction of particles in the suspension, $n$ is the shape factor, and $\psi$ is the sphericity of particles, which was taken as 0.5 due to the non-spherical shape of the particles. Using the above equations, the thermophysical properties of $CrO_2$ and $Fe_2O_3$ suspensions and their fins are calculated as given below:

**Table S1**: Calculated thermophysical properties of $CrO_2$ and $Fe_2O_3$ suspensions [2, 3]

| **Variables** | **DI Water** | **$CrO_2$** | **$Fe_2O_3$** | **$CrO_2$ Suspension** | **$Fe_2O_3$ Suspension** |
|---|---|---|---|---|---|
| Density, ρ ($kg/m^3$) | 998 | 5220 | 5240 | 1049 | 1047 |
| Heat capacity, cp (J/kg.K) | 4200 | 770 | 550 | 3974 | 3969 |
| Thermal conductivity, k (W/mK) | 0.6 | 31 | 6 | 0.0621 | 0.616 |
| Volume fraction, Ø (*v/v*) | -- | -- | -- | 0.012 | 0.0115 |
| Shape factor, *n* | -- | 6 | 3 | -- | -- |
| Viscosity, $\mu$ (Pa.S) | 0.001 | -- | -- | 0.001 | 0.001 |

**Supplementary Information 3: Thermal conductivity of $CrO_2$ and $Fe_2O_3$ nanofins**

Equation (4) can be used for computing the thermal conductivity of nanofins formed using particles of different length-to-width ratios. In this case, $n$ is defined as[1]:

$$n = \frac{3}{\psi} \qquad (5)$$

For which $\psi$ is the sphericity factor. This number is 1 for spherical nanoparticles, and 0.68 and 0.62 respectively for ellipsoidal structures with the aspect ratios of 5:1 and 10:1[4]. The $CrO_2$ particles used in this measurement has a 7:1 ratio that falls between these two values and the sphericity of $Fe_2O_3$ particles is 1. $\psi$ of 0.5 was also included for comparison. The volume fraction concentration of the fins ($\O_{Fin}$) is assumed to be ranging from 10% to 100% for materials forming the nanfins. The range is chosen as we don't know how dense the bundles of the nanofins are. The graphs are shown in Fig. S2. As can be seen, the thermal conductivity of the medium changes from ~0.77 W $m^{-1}$ $K^1$ to 31 W $m^{-1}$ $K^1$ (for $CrO_2$ nanofins) and from ~0.72 W $m^{-1}$ $K^1$ to 6 W $m^{-1}$ $K^1$ (for $Fe_2O_3$ nanofins), when the materials concentration ranges from 10 to 100% (sparse nanofins to very dense nanofins). From these calculations, it is obvious that an elongated morphology such as nano-rod ($CrO_2$) with the aspect ratio of 7:1 (that lies between the 0.62 and 0.68 sphericity graphs) in our case will perform better than any morphology of $F_2O_3$ in heat conduction.

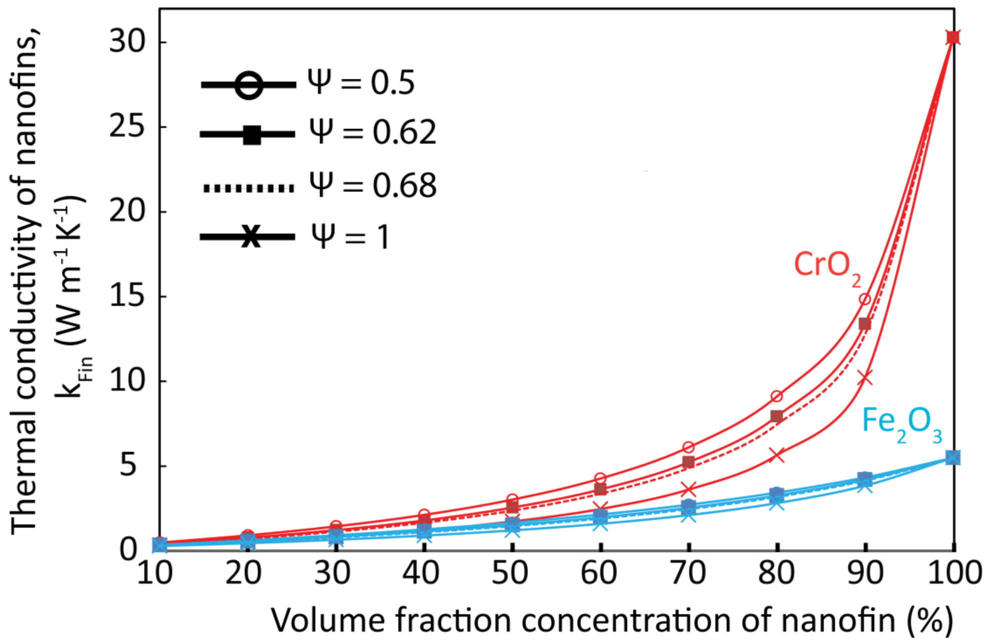


**Fig. S2** Thermal conductivity of $CrO_2$ and $Fe_2O_3$ nanofins under different shapes factors and different concentrations.

**Supplementary Information 4: Size distribution of $Fe_2O_3$ nanoparticles**

Further investigation of heat transfer was conducted with different sizes of $Fe_2O_3$ nanoparticles. The original sample of $Fe_2O_3$ nanoparticle suspension has an average diameter of 184 nm, as confirmed by Dynamic Light Scattering (DLS) (ALV-GmbH, Germany) measurements (Fig. S3). This solution was then been separated using Nylon Syringe Filters of two different sizes: (1) with the porosity of 220 nm and (2) with the porosity of 450 nm. The collected samples had the average diameters of 106 nm and 128 nm, respectively (see Fig. S3). The new samples were centrifuged and diluted to produce the same concentrations (0.06% *w/w)* to the original sample. These new samples were used for further studies of trapping mechanisms and heat transfer efficiency in comparison to the original sample.

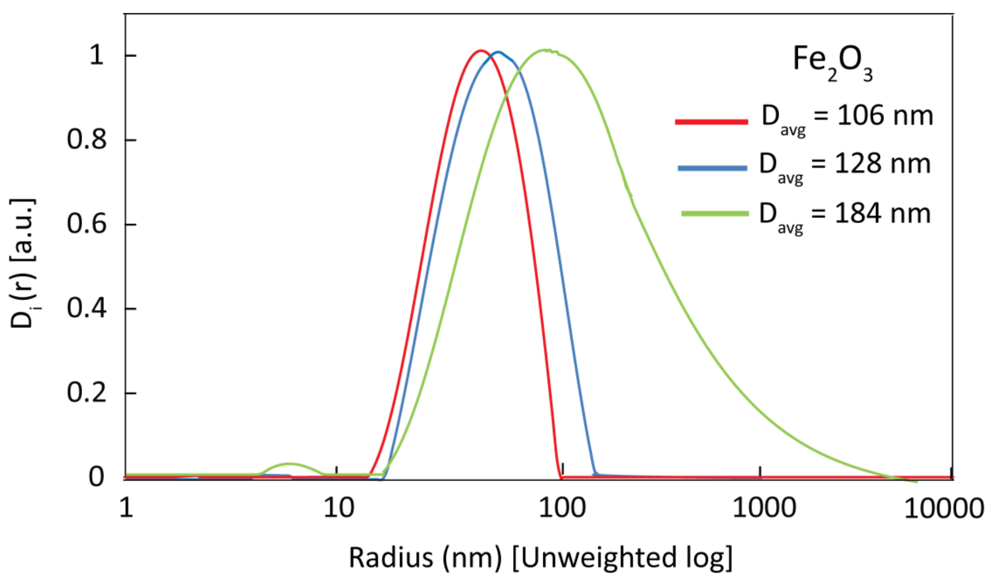


**Fig. S3** Size distribution measurement of $Fe_2O_3$ suspended nanoparticles using a DLS system. The original sample had an average diameter of 184 nm, and the filtered samples were 128 and 106 nm in average diameters, respectively. $D_i(r)$ is the normalized distribution of the particles' concentrations at each radius.

**Supplementary Information 5: Magnetic field strength of the permanent magnets**

The magnetic field effect on the nearby electronic component should be considered. There the field drop measurements from the tip of the magnets were conducted using a Teslameter (F. W. BELL, USA). As can be seen in Fig. S4, the magnetic field drops rapidly to less than 90% of the initial value at 8.1 mm from the source.

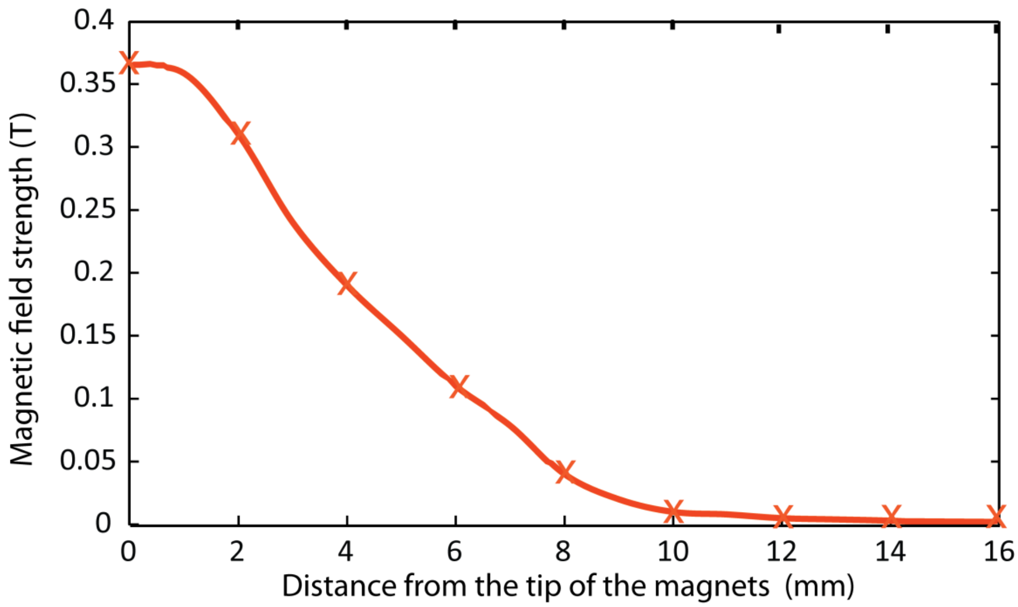


**Fig. S4** The magnetic field strength as a function of the distance from the magnet

## Supplementary Information 6: Trapping characteristics of $Fe_2O_3$ nanoparticles under various flow rates of 10, 40 and 120 µl min$^{-1}$

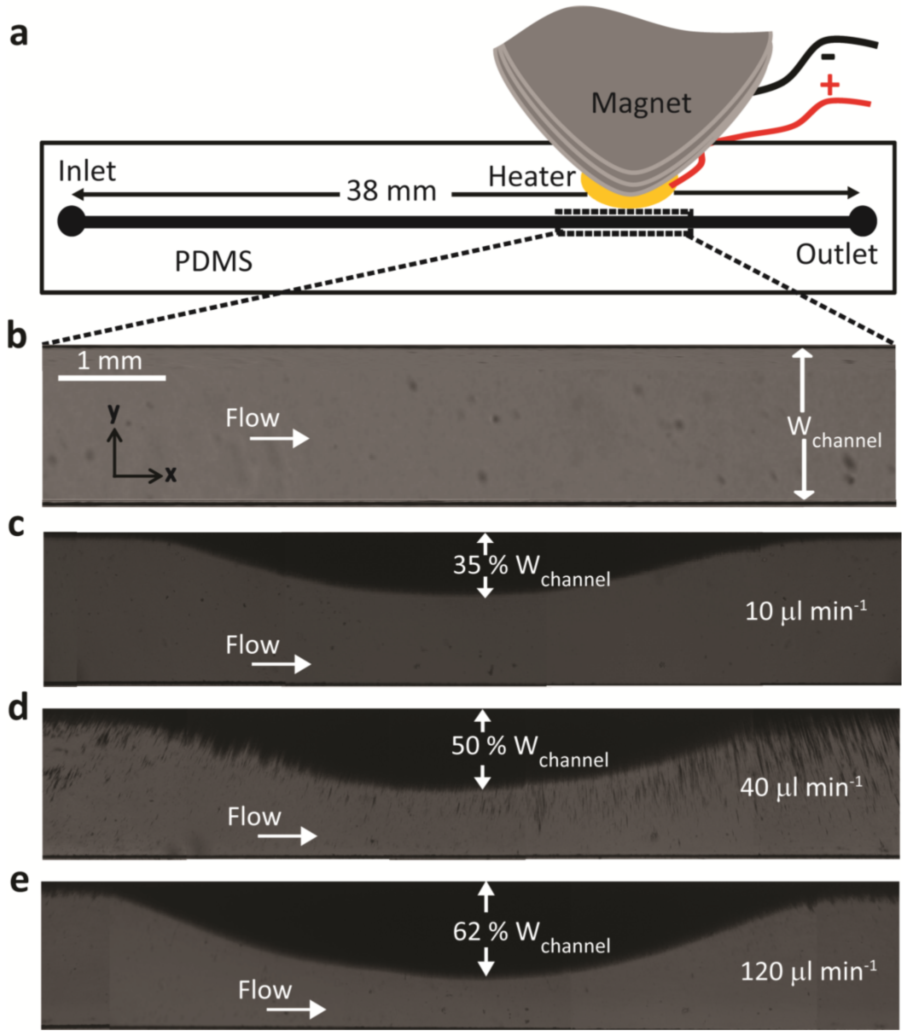


**Fig. S5** Growing length of $Fe_2O_3$ nanoparticle bundles (nanofins) under the influence of the magnetic field at different flow rates of 10, 40, and 120 µl min$^{-1}$, with duration after 10 min. (**a**) A schematic of the microchannel. (**b**) A flow of DI water representing the trapped section of nanoparticles. (**c**) At 10 µl min$^{-1}$ the length of $Fe_2O_3$ fins were obtained to be 35 % of the microchannel's width. (**d**) At 40 µl min$^{-1}$ the length of $Fe_2O_3$ fins were obtained to be 50 % of the microchannel's width. (**e**) At 120 µl min$^{-1}$ the length of $Fe_2O_3$ fins were obtained to be 62 % of the microchannel's width.

**Supplementary Information 7: Thermal characterization of $CrO_2$ nanofins at 10 µl min$^{-1}$**

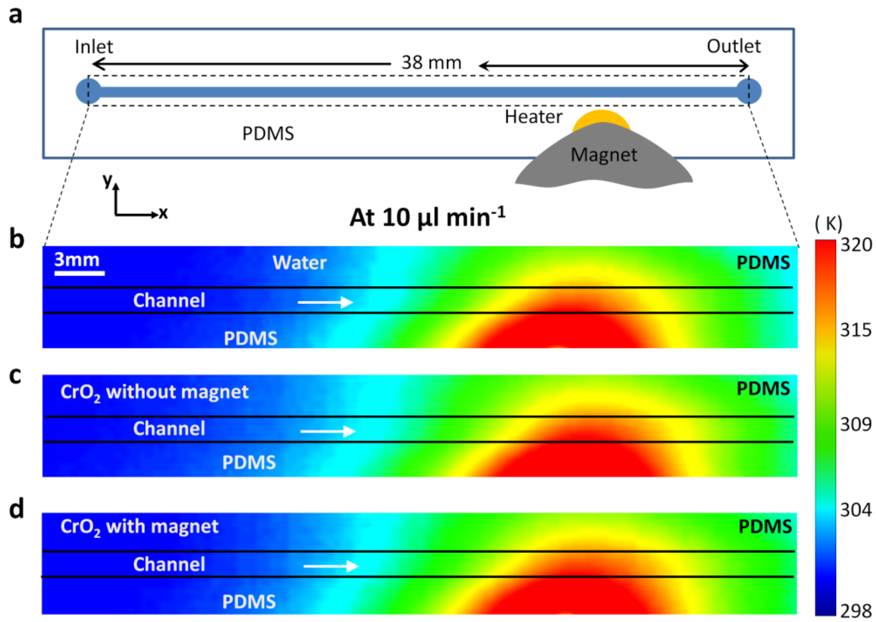


**Fig. S6** Contours of temperature along the glass slide, obtained by infrared camera at a flow rate of 10 µl min$^{-1}$ for the cases of: **(a)** Schematic of microchannel. (**b**) DI water flowing through the microchannel. (**c)** $CrO_2$ nanoparticle suspension in the absence of the magnet. (**d**) $CrO_2$ nanoparticle suspension in the presence of the magnet, leading to formation of $CrO_2$ nanofin along the side wall.

**Supplementary Information 8: Thermal characterization of $Fe_2O_3$ nanofins under various flow rates of 10, 40 and 120 µl min$^{-1}$**

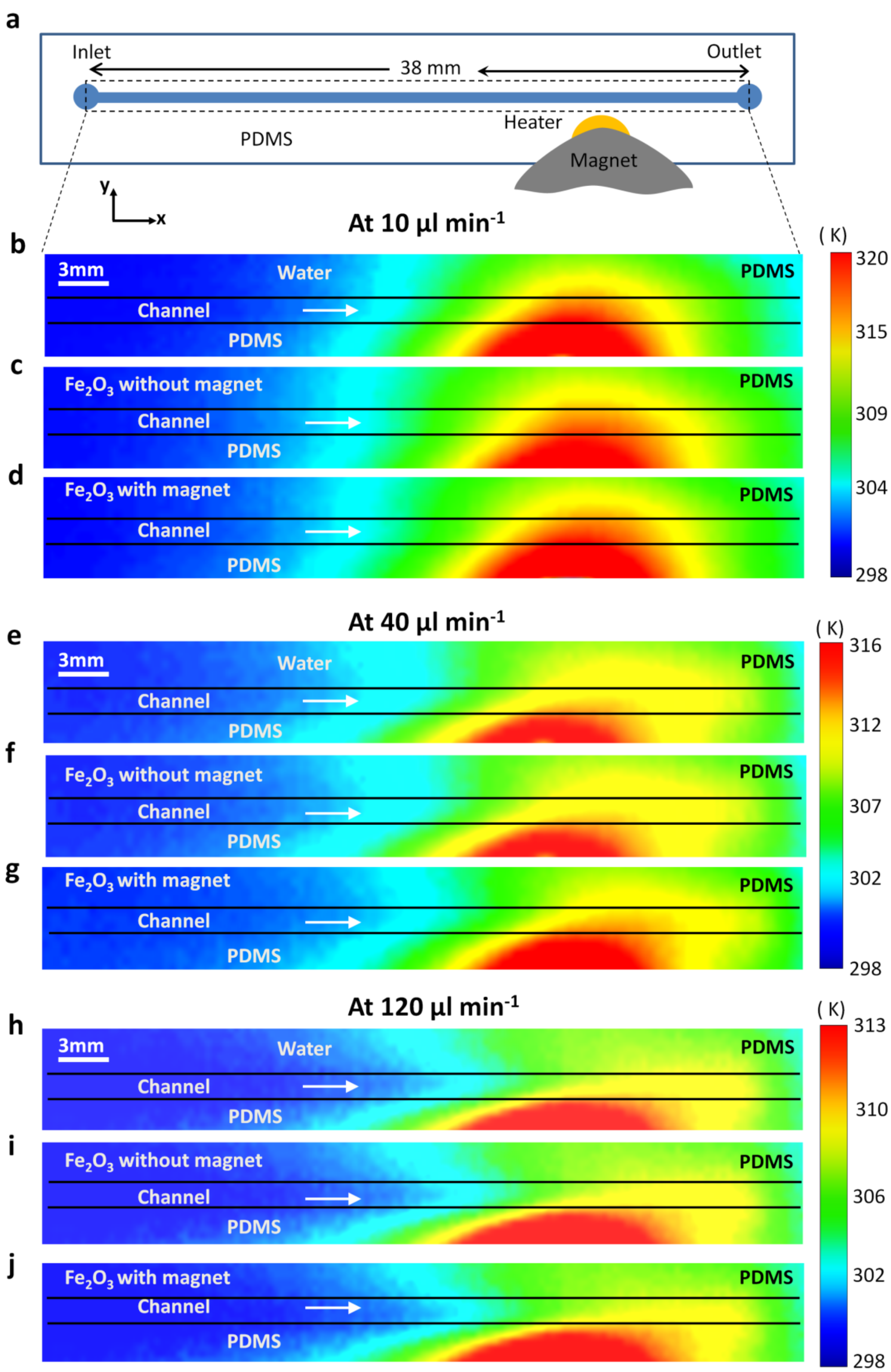

**Fig. S7** Contours of temperature along the glass slide, obtained by infrared camera at a flow rate of 10, 40 and 120 µl $min^{-1}$ for the cases of: (**a**) Schematics of microchannel. At a flow rate of 10 µl $min^{-1}$: (**b)** DI water flows through the microchannel. (**c)** $Fe_2O_3$nanoparticle suspension in the absence of the magnet. (**d**) $Fe_2O_3$nanoparticle suspension in the presence of the magnet, leading to formation of $Fe_2O_3$ nanofin along the side wall. At a flow rate of 40 µl $min^{-1}$: (**e)** DI water flows through the microchannel. (**f)** $Fe_2O_3$ nanoparticle suspension in the absence of the magnet. (**g**) $Fe_2O_3$nanoparticle suspension in the presence of the magnet, leading to formation of $Fe_2O_3$ nanofin along the side wall. At a flow rate of 120 µl $min^{-1}$: (**h)** DI water flows through the microchannel. **(i)** $Fe_2O_3$nanoparticle suspension in the absence of the magnet. (**j**) $Fe_2O_3$ nanoparticle suspension in the presence of the magnet, leading to formation of $Fe_2O_3$ nanofin along the side wall.

**Supplementary Information 9: Effect of narrow microchannel on trapping and thermal studies of $Fe_2O_3$ nanofins at a flow rate of 40 µl min$^{-1}$**

We have conducted experiments with various widths of the microchannel's (1500, 1000 and 500 µm). The results show that reducing the microchannel's width does not increase or decrease the growth rate of nanofins (Fig. S8). Although making the channel smaller facilitates the conductive heat transfer across the channel, it can potentially results in clogging the microchannel.

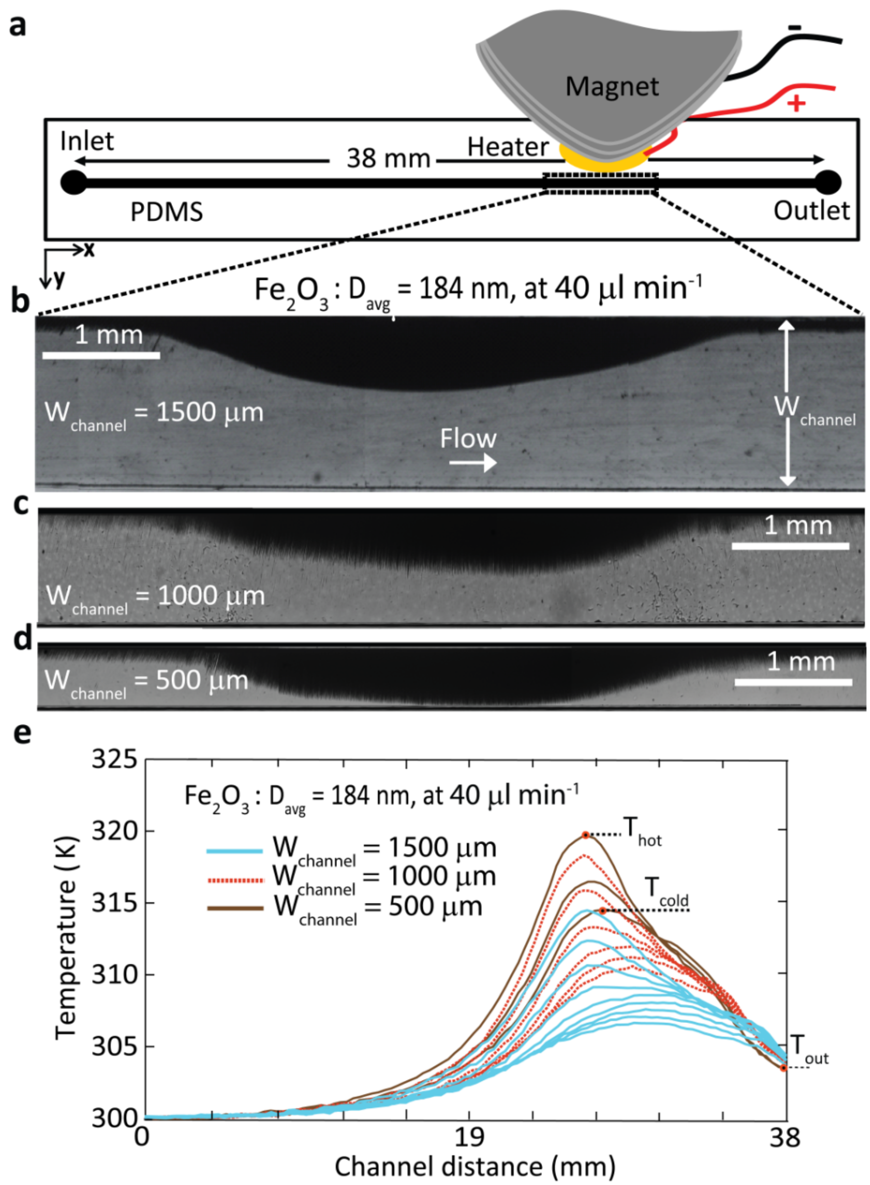

**Fig. S8** Growing length of $Fe_2O_3$ nanoparticle ($D_{avg}$ = 184 nm) bundles (nanofins) under the influence of the magnetic field at a flow rate of 40 µl $min^{-1}$ after 10 min. (**a**) A schematic of the microchannel. The growth of $Fe_2O_3$ nanofins in a microchannel with a width of (**b**) 1500 µm, (**c**) 1000 µm and (**d**) 500 µm, respectively, and (**e**) variations of temperature along the microchannels with various widths at a flow rate of 40 µl $min^{-1}$ (the temperature profiles are taken similar to those of Fig. 5 – 9, 6 and 3 parallel lines for 1500, 1000, and 500 µm cases, respectively)

**Supplementary Information 10: Thermal performance of $CrO_2$ vs. $Fe_2O_3$ nanofins at 10 µl min$^{-1}$**

At a low flow rate of 10 µl min$^{-1}$, the temperature plots follow a bell-shaped configuration, where the peak temperatures in the middle of the bell result from the heat generated at the core of the hot spot (heater), as shown in Fig. S9a. Such configuration implies the dominance of conductive heat transfer at this flow rate. As a result, there is no significant heat transfer improvement even with the addition of nanoparticles nor having nanofin structures of $CrO_2$ or $Fe_2O_3$ nanoparticles.

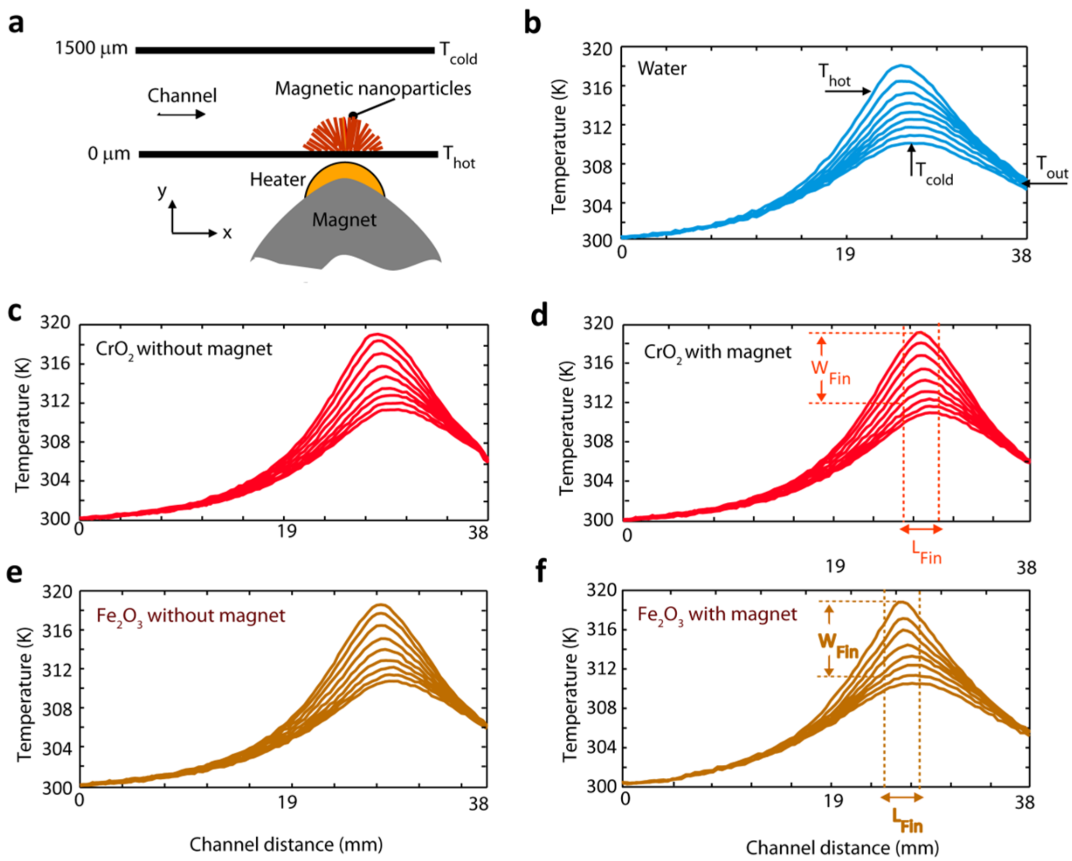


**Fig. S9** Thermal effect of $Fe_2O_3$ and $CrO_2$ nanofins along the microchannel at flow rates of 10 µlmin$^{-1}$: (**a**) Schematic shows trapping particles, (**b**) Water. (**c**) $CrO_2$ nanoparticles suspension without applying the permanent magnet, (**d**) $CrO_2$ nanofins after applying the permanent magnet, (**e**) $Fe_2O_3$ nanoparticles suspension without applying the permanent magnet, and (**f**) $Fe_2O_3$ nanofins after applying the permanent magnet.

## References


1. P. Yi, A. A. Kayani, A. F. Chrimes, K. Ghorbani, S. Nahavandi, K. Kalantar-zadeh and K. Khoshmanesh, *Lab on a Chip*, 2012, **12**, 2520-2525.
2. E. Takegoshi, Y. Hirasawa, S. Imura and a. T. Shimazaki, *International Journal of Thermophysics*, 1984, **5**, 219-228.
3. X. Zhang, Y. Chen, L. Lu and Z. Li, *Journal of Physics-Condensed Matter*, 2006, **18**, L559-L566.
4. R. L. Hamilton and O. K. Crosser, *Industrial & Engineering Chemistry Fundamentals*, 1962, **1**, 187-191.